Experimental confirmation of long-memory correlations in star-wander data

Luciano Zunino,[1,2,*] Damián Gulich,[1,3] Gustavo Funes,[1] and Aziz Ziad[4]

[1]*Centro de Investigaciones Ópticas (CONICET La Plata - CIC), C.C. 3, 1897 Gonnet, Argentina*

[2]*Departamento de Ciencias Básicas, Facultad de Ingeniería, Universidad Nacional de La Plata (UNLP), 1900 La Plata, Argentina*

[3]*Departamento de Física, Facultad de Ciencias Exactas, Universidad Nacional de La Plata (UNLP), 1900 La Plata, Argentina*

[4]*Laboratoire J. L. Lagrange UMR 7293, Université de Nice Sophia-Antipolis/CNRS/OCA, 06108 Parc Valrose, Nice, France*

**Corresponding author: lucianoz@ciop.unlp.edu.ar*

Received April 24, 2014; accepted May 19, 2014;
posted May 22, 2014 (Doc. ID 210726); published June 17, 2014

In this Letter we have analyzed the temporal correlations of the angle-of-arrival fluctuations of stellar images. Experimentally measured data were carefully examined by implementing multifractal detrended fluctuation analysis. This algorithm is able to discriminate the presence of fractal and multifractal structures in recorded time sequences. We have confirmed that turbulence-degraded stellar wavefronts are compatible with a long-memory correlated monofractal process. This experimental result is quite significant for the accurate comprehension and modeling of the atmospheric turbulence effects on the stellar images. It can also be of great utility within the adaptive optics field. © 2014 Optical Society of America

OCIS codes: (000.5490) Probability theory, stochastic processes, and statistics; (010.1290) Atmospheric optics; (010.1300) Atmospheric propagation; (010.1330) Atmospheric turbulence; (010.7350) Wave-front sensing; (350.1260) Astronomical optics.

http://dx.doi.org/10.1364/OL.39.003718

It is well-known that optical waves are strongly affected by the refractive-index fluctuations along the optical path. Because of this phenomenon, the spatial resolution of Earth telescopes is mainly limited by the atmospheric turbulence rather than by the optical design and optical quality [1]. This is the prime reason why the best ground-based sites, with extraordinary stable atmosphere and minimum seeing, are very carefully selected before any large telescopes are placed there. Speckle imaging methods and adaptive optics techniques were introduced to mitigate turbulence-induced phase fluctuations. Furthermore, space telescopes have also been developed as an efficient but too expensive solution to overcome this unwanted drawback.

Performance of ground-based optical astronomy is directly linked to atmospheric conditions. Consequently, accurate modeling of atmospheric turbulence effects is crucial for improving astronomical observations. For example, in adaptive optics systems, atmospherically distorted wavefront predictions could help to decrease wavefront reconstruction errors [2]. Since the wavefront tilt is the dominant atmospheric aberration across the telescope pupil, its statistical characterization turns out to be of paramount importance. Atmospherically distorted images have traditionally been modeled as fully random stochastic processes [3]. Schwartz *et al.* [4] enhanced this idea by identifying turbulence-degraded wavefronts as fractal surfaces. More precisely, the wavefront phase is modeled in the inertial range as a fractional Brownian motion surface with a Hurst exponent $H = 5/6$. This fractal model can be also associated with temporal behavior by assuming the validity of the frozen-flow hypothesis [4]. Fractional Brownian motion (fBm) is a family of Gaussian self-similar stochastic processes with stationary increments [fractional Gaussian noise, (fGn)] widely used for modeling fractal phenomena that have empirical spectra of power-law type $1/f^{\alpha}$ and $\alpha = 2H + 1$ with $1 < \alpha < 3$ [5]. The Hurst exponent $H \in (0, 1)$ quantifies their intrinsic long-range correlations. When $H > 1/2$ consecutive increments tend to have the same sign so that these processes are persistent ([6], Chap. 9). For $H < 1/2$, on the other hand, consecutive increments are more likely to have opposite signs, and it is said that the processes are anti-persistent ([6], Chap. 9). The standard memoryless Brownian motion (random walk) is recovered for $H = 1/2$. Following a different hypothesis, Jorgenson *et al.* [7] suggested that atmospherically induced effects on stellar images may be better modeled by a chaotic deterministic than by a random process. However, a few years later, the same authors concluded in favor of a correlated stochastic dynamic [8] in agreement with the fBm model proposed in [4]. It is worth mentioning that this striking memory effect has been previously confirmed in a more general framework; the propagation of optical waves through disordered media [9].

Taking into account the ubiquity of multifractals in nature, we look for the presence of multiple scaling exponents in the same range of temporal scales for star-wander data. The accurate identification of these scaling exponents is fundamental to develop suitable models for simulation and forecasting purposes. In this Letter the fractal and multifractal nature of experimentally recorded angle-of-arrival (AA) fluctuations of stellar images is examined via multifractal detrended fluctuation analysis (MF-DFA) [10]. This technique is particularly reliable for unveiling the fractal and multifractal scalings in experimental time series. Even though other methods have been proposed for the same purpose, MF-DFA is widely accepted due to its easy implementation and accuracy. Furthermore, it is recommended in the majority of situations in which the multifractal character of data is unknown *a priori* [11].

MF-DFA is based on the traditional DFA method [12], which has been widely proved to be robust, simple, and versatile for accurately quantifying the long-range

correlations embedded in nonstationary time series [13]. Briefly explained, given a time series $S = \{x_t, t = 1, \ldots, N\}$, with N being the number of observations, the cumulated data series

$$Y(i) = \sum_{t=1}^{i} (x_t - \langle x \rangle),$$

with $i = 1, \ldots, N$ and

$$\langle x \rangle = \left(\sum_{t=1}^{N} x_t \right) / N,$$

is considered. This profile is divided into $\lfloor N/s \rfloor$ nonoverlapping windows of equal length s ($\lfloor a \rfloor$ denotes the largest integer less than or equal to a). A local polynomial fit $y_{\nu,m}(i)$ of degree m is fitted to the profile for each window $\nu = 1, \ldots, \lfloor N/s \rfloor$. The degree of the polynomial can be varied to eliminate constant ($m = 0$), linear ($m = 1$), quadratic ($m = 2$), or higher order trends of the profile. Then the variance of the detrended time series is evaluated by averaging over all data points i in each segment ν,

$$F_m^2(\nu, s) = \frac{1}{s} \sum_{i=1}^{s} \{Y[(\nu - 1)s + i] - y_{\nu,m}(i)\}^2,$$

for $\nu = 1, \ldots, \lfloor N/s \rfloor$. In order to analyze the influence of fluctuations of different magnitudes and on different time scales, the generalized qth order fluctuation function given by

$$F_q(s) = \left\{ \frac{1}{\lfloor N/s \rfloor} \sum_{\nu=1}^{\lfloor N/s \rfloor} [F_m^2(\nu, s)]^{q/2} \right\}^{1/q},$$

is estimated for different values of the time scale s and for different values of the order q ($q \neq 0$). When $q = 0$ a logarithmic averaging procedure has to be employed because of the diverging exponent. For $q = 2$, the conventional fractal DFA algorithm is retrieved. Generally, if the time series $S = \{x_t, t = 1, \ldots, N\}$ has long-range power-law correlations, $F_q(s)$ scales with s as

$$F_q(s) \sim s^{h(q)} \tag{1}$$

for a certain range of s. The scaling exponents $h(q)$, usually known as generalized Hurst exponents, are estimated by analyzing the double logarithmic plot of $F_q(s)$ versus s for each value of q. Ideally, if the series is monofractal and stationary, then $h(q)$ is constantly equal to the Hurst exponent H, i.e., independent of q ($h(q) = H$). Otherwise, a multifractal structure is observed when the scaling behaviors of small and large fluctuations are different. In this case the generalized Hurst exponent is a decreasing function of q and the main Hurst exponent can be estimated from the second moment ($h(2) = H$). The generalized Hurst exponents with negative order q describe the scaling of small fluctuations because the segments ν with small variance will dominate the average $F_q(s)$ for this q-range. On the contrary, for positive order q the windows ν with large variance have stronger influence and, thus, the scaling of large fluctuations is examined. The strength of multifractality present in data is usually defined as the spread of the generalized Hurst exponents [14]. As small fluctuations are characterized by larger scaling exponents than those associated with large fluctuations, $h(q)$ for $q < 0$ are larger than those for $q > 0$, and the multifractality degree can be quantified by

$$\Delta h \equiv h(-q) - h(q), \tag{2}$$

for a larger value of the moment q. For further details about MF-DFA and its implementation in MATLAB we recommend [15].

The experimental AA fluctuation measurements were taken by the generalized seeing monitor instrument [16,17] on a star at Paranal Observatory (Antofagasta, Chile). More precisely, 19 independent sets of data recorded on December 16, 2007 were carefully analyzed. The AA fluctuations are measured with a tight and regular sampling of 5 ms during approximately 1 min acquisition time (time series length $N = 11,984$). The data acquisition is repeated typically every 4 min. Figure 1 shows one representative sample of the AA fluctuations (top plot) together with the average temporal power spectral density (PSD) of the 19 sequences (bottom plot). The expected −2/3 power law scaling at the low-frequency region is shown (red-dashed line). The vertical black-dashed line indicates the knee frequency that appears due to the spatial averaging over the telescope aperture [18].

We have analyzed the fractal and multifractal behavior of the AA fluctuations of stellar images by implementing the MF-DFA technique with a detrending polynomial of second order $m = 2$. Similar results were obtained with other orders of the detrending polynomials ($m = 1$, 3, and 4). One hundred time scales $s \in [10, N/4]$ equally distributed in the logarithmic scale were selected for estimating the fluctuation functions. We restrict the moment q to the range $[-20, 20]$ with step equal to 0.25 ($q = -20, -19.75, \ldots, 20$). As an illustrative example, fluctuation functions $F_q(s)$ for the AA fluctuations plotted in

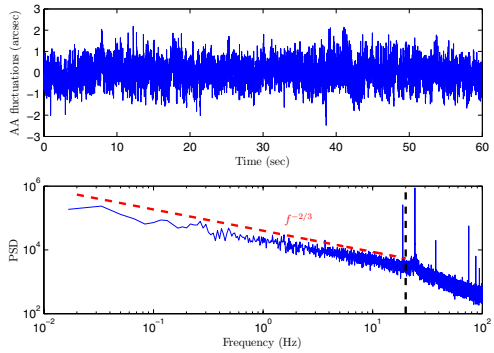

Fig. 1. Representative sample of the AA fluctuations (top) and average PSD of the 19 sequences of real wavefront slopes (bottom). The theoretical expected −2/3 power-law behavior at the low-frequency regime is plotted (red-dashed line). The knee frequency is also indicated (vertical black-dashed line). Peaks observed at high frequencies are due to vibrations in the experimental arrangement.

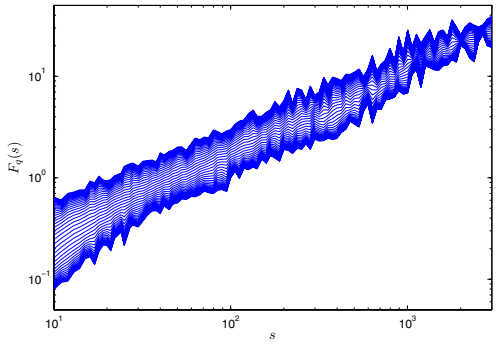

Fig. 2. Fluctuation functions $F_q(s)$ as a function of the scale s for the AA fluctuations plotted in Fig. 1. A detrending polynomial of order $m = 2$ and 100 different scales $s \in [10, N/4]$ equally spaced in the logarithmic scale were employed in the MF-DFA implementation. The order q ($q = -20, -19, \ldots, 20$) increases from bottom to top. The behavior observed is representative for the whole data set.

Fig. 1 are shown in Fig. 2. Only $F_q(s)$ with integer moment, i.e., $q = -20, -19, \ldots, 20$, are depicted for a better visualization. From this figure it can be concluded that the slope of the fluctuation functions in the log–log plot, $h(q)$, slightly decrease with the moment q.

To better understand the fractal nature, Fig. 3 shows the fluctuation function for the second moment $F_2(s)$ as a function of the scale s for the 19 independent sets of AA fluctuations. The excellent linearity observed for all the time scales should be emphasized. This finding allows us to confirm the existence of a well-defined power-law behavior, $F_2(s) \sim s^{h(2)} = s^H$, and, accordingly, a fractal dynamic in the full analyzed range.

Generalized Hurst exponents estimated in the full time scale range, i.e., fitting range $s \in [10, N/4]$, for the 19 independent sets of AA fluctuations are plotted in Fig. 4. The main Hurst related exponents ($H = h(2)$) are indicated with a vertical black continuous line. Values estimated for this parameter (H), together with those obtained for the multifractal strength (Δh), defined according to Eq. (2), are detailed in Fig. 5. Mean and standard deviation of the estimators of both quantities, namely Hurst exponent H and multifractality strength Δh, over the whole data set are 0.79 ± 0.03 and 0.21 ± 0.06, respectively. On the one hand, a persistent

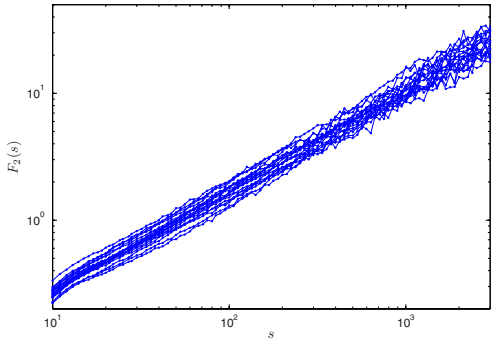

Fig. 3. Fluctuation functions $F_2(s)$ as a function of the scale s for the 19 independent sets of AA fluctuations. The slope of the best linear fit obtained for each one of these fluctuation functions is the Hurst exponent estimator (standard DFA technique [12]) of the experimental records.

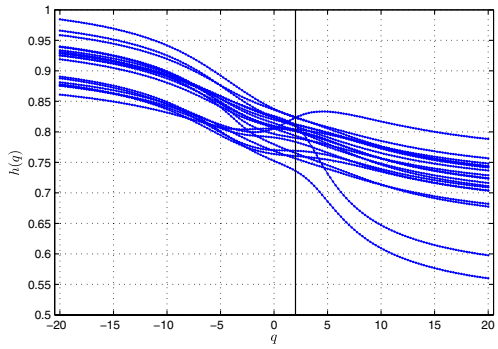

Fig. 4. Generalized Hurst exponents $h(q)$, estimated in the full fitting range $s \in [10, N/4]$, as a function of the order q for the 19 independent sets of AA fluctuations. The vertical black continuous line indicates the estimated values for the main Hurst exponent ($H = h(2)$).

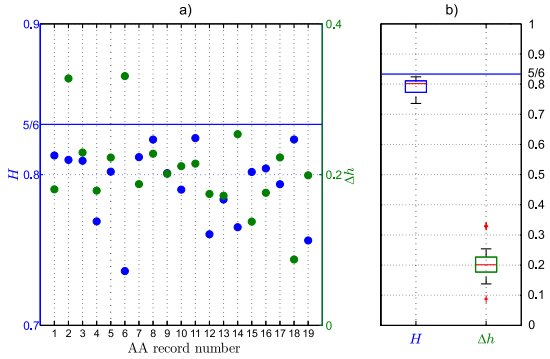

Fig. 5. (a) Estimated values for the Hurst exponent H (blue dots) and multifractality degree Δh (green dots) for the nineteen independent experimental sets of AA fluctuations. (b) Related boxplots for both quantifiers. The theoretical expected value for the Hurst exponent within the Kolmogorov model ($H = 5/6$) is indicated (horizontal blue continuous lines).

stochastic behavior is concluded from the DFA analysis. On the other hand, the results obtained for the generalized Hurst exponents suggest a small degree of multifractality. This small spread of the $h(q)$ values can be directly ascribed to finite-size effects. More precisely, an apparent, false, multifractality degree $\Delta h \approx 0.2$ is commonly found in purely long-range correlated monofractal signals [19]. As it has been proved by Grech and Pamuła [14], this spurious effect appears as a result of finite length of analyzed data and is additionally amplified by the presence of long-term memory. In order to better clarify this issue we have estimated the generalized Hurst exponents of 100 independent realizations of fGn with the Hurst exponent $H = 0.8$. These numerical simulations, with the same length N of the AA fluctuation time series were generated via the function wfbm of MATLAB. This algorithm simulates fBm following the method proposed by Abry and Sellan [20]. The fGn numerical realizations are obtained through successive differences of the fBm simulations. MF-DFA with the same parameters used for the AA fluctuation records was implemented for this numerical study. Mean and standard deviation of the estimated values for H and Δh are 0.80 ± 0.02 and 0.16 ± 0.03, respectively. These results confirm

the existence of a spurious multifractality in monofractal long-range correlated time series due to finite-size effects. Consequently, AA fluctuations of stellar images can be modeled, at least in a first approximation, as a monofractal long-memory correlated stochastic process.

Our experimental results support the fBm model for the atmospherically induced wavefront degradations proposed by Schwartz *et al.* [4]. The estimated Hurst exponent, however, is always below the 5/6 value expected for a conventional Kolmogorov theory. This smaller Hurst exponent can be ascribed to a non-Kolmogorov behavior of the atmospheric turbulence because there exist evidence of deviations from the Kolmogorov model in the upper atmosphere [21,22]. Indeed, Du *et al.* [23] have theoretically found that the power law of the temporal power spectra of AA fluctuations for low frequencies is modified when a generalized power-spectrum model for the refractive-index fluctuations, i.e., non-Kolmogorov turbulence, is considered. This change in the scaling law for the low-frequency regime can be directly associated with the deviations from the Kolmogorov-expected Hurst exponent that we have experimentally observed.

Summarizing, we have confirmed the presence of long-range correlations in AA fluctuations of stellar wavefronts propagating through atmospheric turbulence. The estimated Hurst exponent is always near but below the theoretically expected 5/6 value for a Kolmogorov turbulence. Indeed, this smaller estimated Hurst exponent can be understood in terms of a non-Kolmogorov turbulence model. It is worth emphasizing that these results allow us to suggest that the turbulence-degraded wavefront phase can be modeled as a fBm with $H \approx 0.8$. The inherent predictability associated with this persistent stochastic process might be useful to improve the performance of high-angular-resolution techniques. Further analysis with a larger database is planned for optimizing the Hurst exponent estimation.

This work was partially supported by Consejo Nacional de Investigaciones Científicas y Técnicas (CONICET), Argentina and Universidad Nacional de La Plata (UNLP), Argentina.

References

1. M. C. Roggemann and B. Welsh, *Imaging Through Turbulence* (CRC Press, 1996).
2. M. B. Jorgenson and G. J. M. Aitken, Opt. Lett. **17**, 466 (1992).
3. J. W. Goodman, *Statistical Optics* (Wiley, 1985).
4. C. Schwartz, G. Baum, and E. N. Ribak, J. Opt. Soc. Am. A **11**, 444 (1994).
5. B. B. Mandelbrot and J. W. Van Ness, SIAM Rev. **10**, 422 (1968).
6. J. Feder, *Fractals* (Plenum, 1988).
7. M. B. Jorgenson, G. J. M. Aitken, and E. K. Hege, Opt. Lett. **16**, 64 (1991).
8. D. R. McGaughey and G. J. M. Aitken, J. Opt. Soc. Am. A **14**, 1967 (1997).
9. I. Freund, M. Rosenbluh, and S. Feng, Phys. Rev. Lett. **61**, 2328 (1988).
10. J. W. Kantelhardt, S. A. Zschiegner, E. Koscielny-Bunde, S. Havlin, A. Bunde, and H. E. Stanley, Phy. A **316**, 87 (2002).
11. P. Oświęcimka, J. Kwapień, and S. Drożdż, Phys. Rev. E **74**, 016103 (2006).
12. C.-K. Peng, S. V. Buldyrev, S. Havlin, M. Simons, H. E. Stanley, and A. L. Goldberger, Phys. Rev. E **49**, 1685 (1994).
13. J. W. Kantelhardt, E. Koscielny-Bunde, H. H. A. Rego, S. Havlin, and A. Bunde, Phys. A **295**, 441 (2001).
14. D. Grech and G. Pamuła, Phys. A **392**, 5845 (2013).
15. E. A. F. Ihlen, Front. Physiol. **3**, 141 (2012).
16. A. Ziad, R. Conan, A. Tokovinin, F. Martin, and J. Borgnino, Appl. Opt. **39**, 5415 (2000).
17. A. Ziad, J. Borgnino, W. Dali Ali, A. Berdja, J. Maire, and F. Martin, J. Opt. **14**, 045705 (2012).
18. J.-M. Conan, G. Rousset, and P.-Y. Madec, J. Opt. Soc. Am. A **12**, 1559 (1995).
19. A. Y. Schumann and J. W. Kantelhardt, Phys. A **390**, 2637 (2011).
20. P. Abry and F. Sellan, Appl. Comput. Harmon. Anal. **3**, 377 (1996).
21. D. Dayton, B. Pierson, B. Spielbusch, and J. Gonglewski, Opt. Lett. **17**, 1737 (1992).
22. T. W. Nicholls, G. D. Boreman, and J. C. Dainty, Opt. Lett. **20**, 2460 (1995).
23. W. Du, L. Tan, J. Ma, and Y. Jiang, Opt. Express **18**, 5763 (2010).